Thermally induced mass transfer between nanobubbles and micropancakes

Kimura, Ryota
Department of Aeronautics and Astronautics, Kyushu University

Teshima, Hideaki
Department of Aeronautics and Astronautics, Kyushu University

Li, Qin-Yi
Department of Aeronautics and Astronautics, Kyushu University

Takahashi, Koji
Department of Aeronautics and Astronautics, Kyushu University

出版情報：International Journal of Heat and Mass Transfer. 181, pp.122001-, 2021-12. Elsevier
バージョン：
権利関係：

Thermally Induced Mass Transfer between Nanobubbles and Micropancakes

Ryota Kimura[a], Hideaki Teshima[a,b], Qin-Yi Li[a,b], and Koji Takahashi[a,b,*]

[a]*Department of Aeronautics and Astronautics, Kyushu University, Nishi-Ku, Motooka 744, Fukuoka 819-0395, Japan*

[b]*International Institute for Carbon-Neutral Energy Research (WPI-I2CNER), Kyushu University, Nishi-Ku, Motooka 744, Fukuoka 819-0395, Japan*

*Corresponding author.

E-mail: takahashi@aero.kyushu-u.ac.jp (K. Takahashi)

Abstract

The response of nanoscopic gas phases at solid–liquid interfaces to temperature changes remains unclear. We investigated the interactions between surface nanobubbles and underlying micropancakes upon heating. By atomic force microscopy imaging of the same area before and after heating, we found that the surface nanobubbles exhibited various behaviors upon heating: nucleation, growth, and disappearance. The differences in behavior are attributable to the existence of underlying gas phases, such as micropancakes and adsorbed layers. The nucleation sites of the nanobubbles depend on the positions of the micropancakes. The size of the underlying micropancakes is central to the manner of gas transport between the micropancakes and overlying nanobubbles. We propose that the strongly adsorbed gas layers attract dissolved gas molecules and thereby lead to irreversible growth before and after heating.

Keywords

Nanobubble; Micropancake; Adsorbed layer; Heat transfer; Atomic force microscopy

1. Introduction

Nanoscale bubbles at the solid–liquid interface exhibit various interrelated interfacial phenomena, such as the onset of nucleate boiling with low superheating or even below the boiling point[1,2], fluid slippage and concomitant drag reduction[3–5], long-range hydrophobic interactions between in-water surfaces[6,7], and stabilization of water films in nanoscale spaces under vacuum[8]. Surface nanobubbles have unique characteristics—such as a flat shape and long lifetime[9]—that cannot be explained by traditional theories and exhibit superstability against disturbances[10,11]. To explain these characteristics, researchers have proposed a variety of theories, such as contamination theory[12], dynamic equilibrium theory[13,14], and contact line pinning and gas supersaturation[15]. Surface nanobubbles coexist with micropancakes, which spread laterally for several hundred nanometers or even micrometers with a uniform thickness of several nanometers[16–21], and thinner layers composed of adsorbed gas molecules. These thinner layers consist of (1) an ordered layer that is several molecules thick and exhibits a row-like structure that is influenced by the crystal structure of the substrate[22] and (2) a disordered layer that covers the ordered layer[23].

Heat transfer researchers have begun to recognize the pertinence of surface nanobubbles; specifically, the relationship between surface nanobubbles and the initial stage of boiling phenomena. For phase change cooling systems for electronics, the quick start of nucleate boiling is highly desired to prevent the electronic components from

thermal shocks associated with superheating. Macroscopic experiments indicate that bubble nuclei trapped in geometrical cavities act as boiling nuclei in the initial stage of boiling[24–27]. However, one cannot explain all experimental results by such traditional models. For example, Nam and Ju[1] observed nucleate boiling with low superheating on a nanoscopically smooth hydrophobic surface and proposed that surface nanobubbles act as boiling nuclei. Shen et al.[2] attributed the onset of nucleate boiling below the boiling point on a biphilic surface to surface nanobubbles that form on hydrophobic spots. These results indicate that dissolved gas molecules and surface nanobubbles are strongly related to the onset of nucleate boiling and have a potential to initiate it at extremely low temperature. Therefore, to understand the detailed mechanism of initial stage of boiling and to enable the design of an optimized heating surface that considerably suppresses the superheating, one must investigate the response of surface nanobubbles to temperature changes.

Although some studies have reported the responses of nanobubbles to temperature changes[1,28–32], there is no unified understanding of underlying mechanisms. For example, Yang et al.[28] reported that nanobubbles spontaneously form during heating and did not disappear after heating. Berkelaar et al.[30] reported that some bubbles grew but others shrank when the temperature decreased from a value of 51°C to a value of 25°C. Furthermore, in contrast to the results of Nam and Ju[1] and Shen et al.[2], some reports indicate that surface nanobubbles do not grow into large bubbles even when heated to temperatures close to the boiling point[29,32]. These disparate results may be due to the lack of simultaneous investigations of nanobubbles and the underlying gas phases.

In this study, we achieved the following: (1) simultaneously observed surface

nanobubbles, micropancakes, and a disordered layer on a highly oriented pyrolytic graphite (HOPG)/pure water interface; and (2) measured changes induced by heating. The size of the micropancakes was central to growth of the overlying nanobubbles. Our results will help researchers understand how the gas phase at the solid–liquid interface behaves in response to heating and further improve knowledge of phase-change heat transfer.

2. Experimental

An HOPG substrate (SPI-1 grade, 10 mm × 10 mm, Alliance Biosystems, Japan) was fixed by applying epoxy adhesive EPO-TEK 377 (Epoxy Technology, Inc., USA) to its back side, which was placed on the bottom of a glass liquid cell (approximately 5-mm depth) and baked at 150°C for 1 h. This two-component adhesive does not use any solvents and does not dissolve, even in alcohol. Before measurement, the entire liquid cell was cleaned with ethanol and pure water and peel off the top surface of the HOPG substrate to afford a fresh surface. The details of the used liquid cell can be found in supplementary note 1. The interfacial nanoscale gas phase was generated by solvent exchange method as it is most often used to nucleate nanobubbles[33]. Specifically, HOPG is immersed in ethanol for a few minutes and then replace with pure water. This exchange creates an air-supersaturated condition in water, resulting in the nucleation of interfacial gas phases. It needs to be noted that this method has not yet been optimized to control the nanobubble nucleation[34] because of the uncontrollability of gas oversaturation. To prevent contamination, clean glass syringes and steel needles were used[35]. Pure water was generated by using a water purifier (RFP742HA, Advantec, Japan). Note that we have confirmed in previous studies[21,36] that the nucleated domains are gas phases and not contamination. Figure 1 shows a diagram of the

experimental system.

For the experiments, the amplitude modulation (AM) mode of a scanning probe microscope (SPM; SPM-8100FM, Shimadzu Corp., Japan) was used and a SCANASYST Fluid+ (Bruker Corp., USA; tip radius, 2–10 nm; resonant frequency, 100–200 Hz; spring constant, 0.35–1.4 N/m) was used for the cantilever. Because hydrophilic cantilevers are preferable for measurements of gas phases in liquid[37], the cantilevers were hydrophilized by O_2 plasma (150 W, 30 min; Plasma Reactor 500, Yamato Scientific, Japan).

The liquid cell was fixed on the heating unit with silver paste and then the sample was heated with a ceramic heating unit (Shimadzu Corp., Japan) that was attached to the scanner top. The water temperature was monitored with a resistance thermometer. After atomic force microscopy (AFM) measurements of the solid–liquid interface at room temperature, the water temperature was increased to either 45°C, 60°C, or 70°C. When the water temperature stabilized, heating was discontinued and AFM measurements were conducted upon a return to room temperature. Figure S2 (supplementary information) shows the cooling rate. All measurements were carried out after a complete cooldown of the surface. Although we have tried to measure the nanobubbles during heating or cooling, the thermal convection induced by the temperature gradient inside the liquid cell prevents us from acquiring the AFM images. We could not conduct the AFM measurement even when the water temperature stabilizes at a high temperature, which may be due to the small thermal fluctuation caused by the conduction and water evaporation.

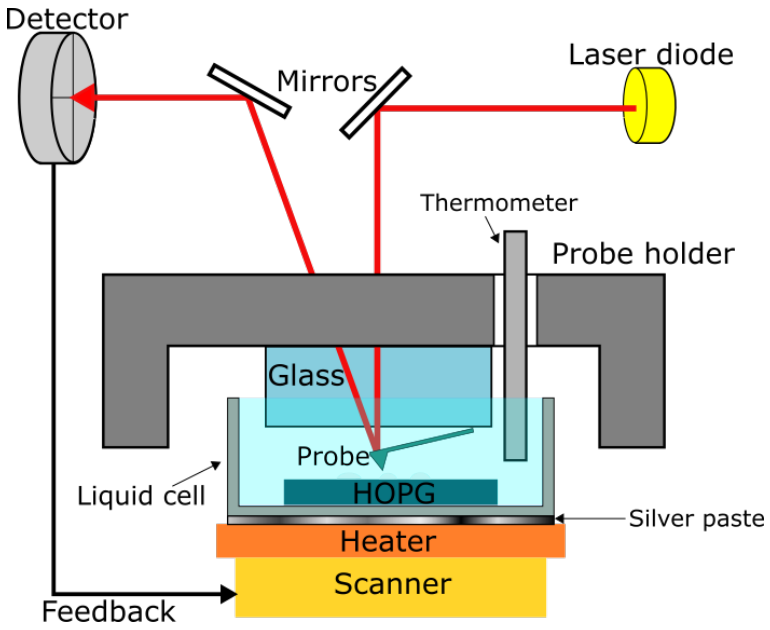

Figure 1 Schematic of the experimental setup for AFM observations in water.

3. Results and discussion

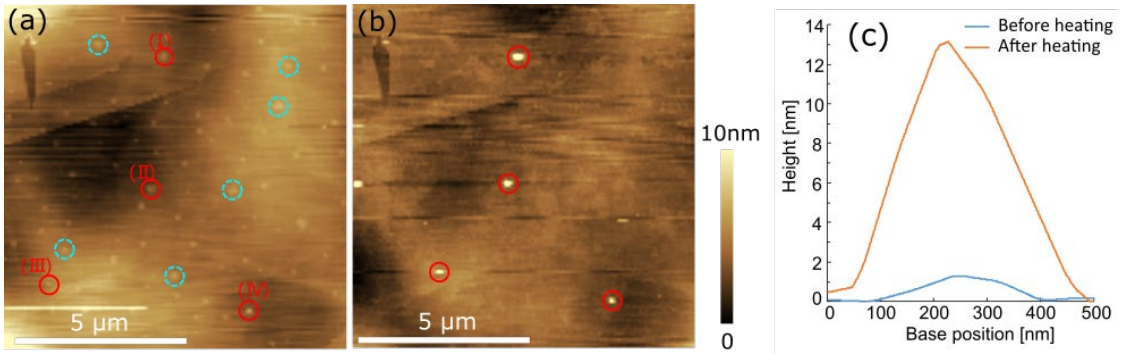

Figure 2 AFM height images of the HOPG/pure water interface: (a) before heating (room temperature), and (b) after heating to 60°C. We acquired both images at room temperature. Red solid circles and blue dotted circles indicate where nanobubbles grew after heating and where nanobubbles were no longer evident after heating, respectively. (c) Cross-sections of the grown nanobubble indicated by the red solid circle (I) before and after heating. The cross-sections of the nanobubbles (II)-(IV) are shown in Figure S3.

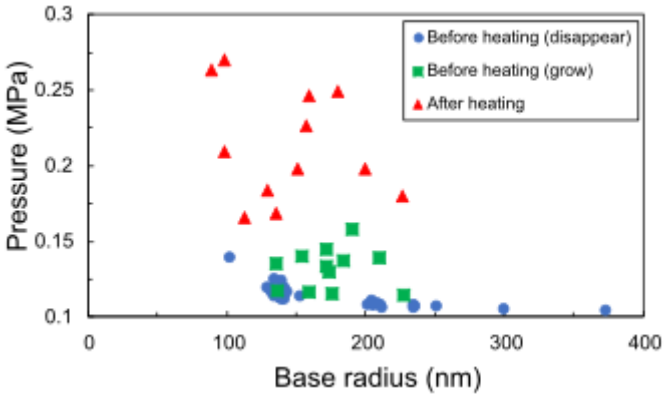

Figure 3 Base radius of nanobubbles versus inner pressure estimated by the Young–Laplace equation $p = (2\gamma / R_c) + p_{atm}$. Here, p is the inner pressure of the bubble, and p_{atm} is the atmospheric pressure. $R_c = r / \sin\theta$ is the radius of curvature, $\theta = \pi - 2 \arctan (h / r)$ is contact angles, and r and h are the base radius and height of the surface nanobubbles, respectively. γ is assumed as 72 mN/m. Blue circle and green squares indicate nanobubbles that were no longer evident after heating and nanobubbles that grew upon heating, respectively. Red triangles indicate nanobubbles that remained after heating. The uncertainty of the base radius and inner pressure values are estimated to be ±1~3.5 % and ±1~4 % for the 95 % confidence interval.

Figure 2 shows AFM height images of the same area measured before heating [Figure 2 (a)] and after heating [Figure 2 (b)]. We observed many surface nanobubbles of base radius ~300 nm over the entire surface. As indicated by blue dotted circles, most of the nanobubbles that were present before heating were no longer evident after heating. However, the nanobubbles indicated by red solid circles remained after heating and all of them grew in height (as shown in Figure 2(c) and Figure S3). More specifically, we observed 44 nanobubbles in Figure 2(a) and 32 nanobubbles disappeared (73 %) and 12 grew (27 %) out of 44 after heating (Figure 2(b)). Table S2 (shown in supplementary note

2) shows the properties of these grown bubbles before and after heating and indicates the tendency that the nanobubbles grew in height, which leads to an increment of the inner pressure. One would commonly presume simultaneous growth and shrinkage of bubbles to be attributable to Ostwald ripening, in which gas molecules are transported from large nanobubbles with higher inner pressure to small ones with lower inner pressure to make the whole system more thermodynamically stable[38,39]. However, nanobubbles that shrank after heating had comparatively lower inner pressures (Figure 3). Therefore, one cannot explain the aforementioned growth and shrinkage by Ostwald ripening.

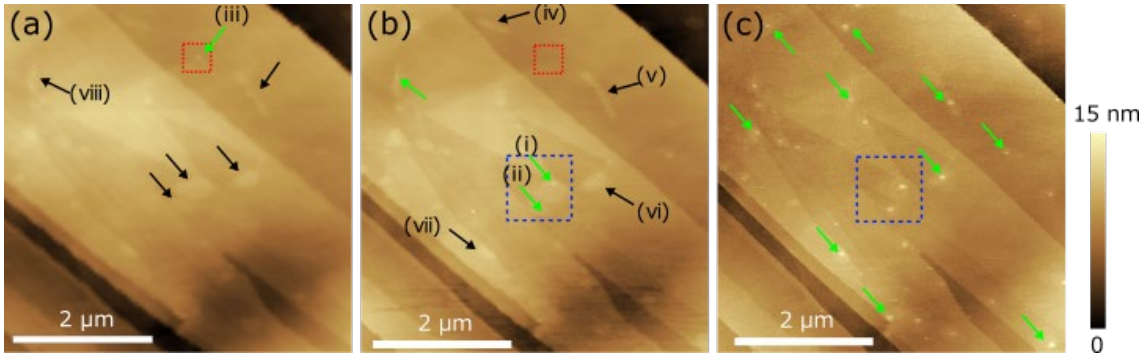

Figure 4 AFM height images of the HOPG/pure water interface: (a) before heating (room temperature), (b) after heating to 45°C, and (c) after heating to 70°C. We measured these images in the same area. Blue dotted frames and red solid frames correspond to the areas shown in Figure 5 (a, b) and Figure 5 (c, d), respectively. Black arrows indicate the micropancakes. Green arrows indicate the nanobubbles on the micropancakes.

To investigate the growth/shrinkage of heated nanobubbles, we conducted other AFM measurements before and after sequential heating within a relatively small area. Figure 4 shows the AFM height images before heating [Figure 4 (a)], after heating to 45°C [Figure 4 (b)], and after heating to 70°C [Figure 4 (c)]. In Figure 4 (a), there are few

nanobubbles and some regions—specifically, the micropancake—are taller than the substrate (black arrows). Although only a few nanobubbles were generated on micropancakes after heating to 45°C [Figure 4 (b)], many of the nanobubbles were then generated on micropancakes (green arrows) when heated to 70°C [Figure 4 (c)]. Moreover, nucleation of the nanobubbles occurred only on the micropancakes, not on the bare HOPG surface. Such a structure in which nanobubbles coexist on a micropancake is termed a nanobubble-on-micropancake[18,19]. Furthermore, we also observed growth and disappearance of nanobubbles after heating, as indicated by the blue and red dotted frames in Figure 4. It should be noted that the micropancakes may exist under the nanobubbles in Figure 2 but could not be precisely imaged because of the low lateral resolution and/or the different conditions of the AFM tip.

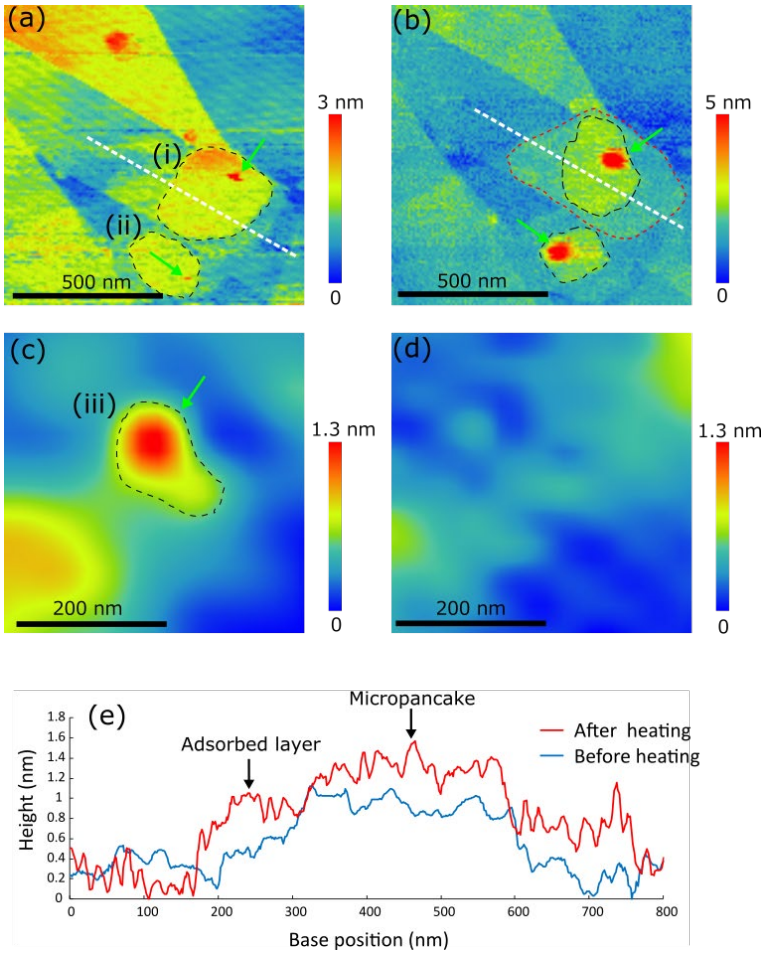

Figure 5 Magnified images of the micropancakes and nanobubbles: (a, c) before heating, and (b, d) after heating. (a, b) and (c, d) correspond to the blue and red dotted frames shown in Figure 4, respectively. Dotted black and red lines indicate the contour of the micropancakes and adsorbed layer, respectively. Arrows indicate the nanobubbles. In (i) and (ii), nanobubbles on the micropancakes grew by heating, yet in (iii) a nanobubble-on-micropancake was no longer evident after heating. (e) Cross sections corresponding to the white dotted lines in (a) and (b), indicating growth of the micropancake and the adsorbed layer.

Table 1 Area and height of gas domain, which contains nanobubbles (NBs) and micropancakes (MPs). The ratio NB/MP is the area of the nanobubbles divided by the area of the micropancakes. The numbers (i), (ii), and (iii) correspond to the same numbers in Figure 4 and 5. The uncertainty of the height and area values is estimated to be ±4~16 % and ±1~8 % for the 95 % confidence interval.

		(i)		(ii)		(iii)	
		NB	MP	NB	MP	NB	MP
Before Heating	Height [nm]	2.0	0.8	1.5	0.7	1.2	0.6
	Area [nm^2]	1500	87900	900	39800	1700	3900
	NB/MP [%]	1.7		2.2		43	
After heating	Height	6.0	1.3	4.9	1.1	-	-
	Area [nm^2]	7400	64800	7800	28200	-	-
	NB/MP [%]	11		28		-	

Figure 5(a, b) shows growth of nanobubble-on-micropancakes (micropancakes marked in black dotted lines) that correspond to the blue dotted frame in Figure 4. Table 1 shows the properties of each gas phase. The area of the micropancakes clearly decreased, although the nanobubbles grew both in height and base radius (Table 1). As a result, the area ratio of the nanobubbles to the micropancakes considerably increased after heating. The same tendency was observed in the different nanobubble-on-micropancake numbered as (viii) in Figure 4 (The detail is shown in Figure S4 and Table S3 in supplementary note 3). Thus, we could observe the respective formation, growth, and disappearance of nanobubbles on micropancakes 30 times, 3 times, and once in Figure 4. Moreover, we also observed a disordered layer under the micropancakes after heating [Figure 5(b), red dotted line]. This is consistent with previous reports that interfacial gases can form multiple layers[19] and that heating increases the thickness of the unaligned layer and renders it detectable by AM–AFM[40]. Next, we focus on Figure 5(c, d). There was a

nanobubble-on-micropancake (Table 1) before heating [Figure 5(c)], and the ratio of the area of the nanobubble to the micropancake was much larger than that discussed previously (Table 1). After heating, neither the nanobubble nor the micropancake were evident [Figure 5(d)].

First, we discuss the nucleation sites of the nanobubbles upon heating. The nanobubbles nucleated only on the previously formed micropancakes and no nanobubbles were generated on the bare HOPG surface (Figure 4). The location where the nanobubbles form has been thought to be related to inhomogeneity and wettability of the surface[41,42]. However, we newly found that nanobubbles are selectively generated on micropancakes. Moreover, new micropancakes and nanobubbles did not form on the bare HOPG surface by heating. This may be because the evolution of gas molecules from water to the pre-existed micropancakes is thermodynamically more favorable than nucleation of new micropancakes or nanobubbles beyond the energy barrier for heterogeneous nucleation.

Table 2 Area and height of micropancakes and nanobubbles which were generated on the micropancakes. The numbers (iv)-(vii) correspond to the same numbers in Figure 4 and S5. The uncertainty of the height and area values is estimated to be ±6~22 and ±1~12 % for the 95 % confidence interval.

		(iv)	(v)	(vi)	(vii)
Area [nm^2]	45 °C	73000	114700	118800	65700
	70 °C	56400	62200	77100	55800
Height [nm]	45 °C	0.8	0.8	1.3	0.9
	70 °C	0.9	1.1	1.2	0.9

We also discuss the nucleation of a nanobubble-on-micropancake. Because the micropancakes are very thin, the gas molecules constituting the micropancakes are strongly attracted by van der Waals forces from the underlying adsorbed layer and HOPG surface. Moreover, because the gas phases near the HOPG surface have a considerably high density[20], their gas–liquid interfacial tension should be much weaker than the macroscopic interfacial tension. Therefore, the micropancake does not instantaneously become semispherical but instead grows while maintaining its flat shape during heating. When its height increases to an extent where thermal fluctuation creates a region where the gas–liquid interfacial tension becomes more dominant than van del Waals forces, a semispherical nanobubble is generated on the micropancake. Furthermore, Table 2 shows the area and height of micropancakes where nanobubbles nucleated before and after heating [in Figure 4 and Figure S5 (supplementary note 4)]. In all cases, the area of the micropancakes became smaller as the nanobubbles formed on them. This result implies that the nucleation and growth consume the underlying micropancakes and thus eventually extinguish them.

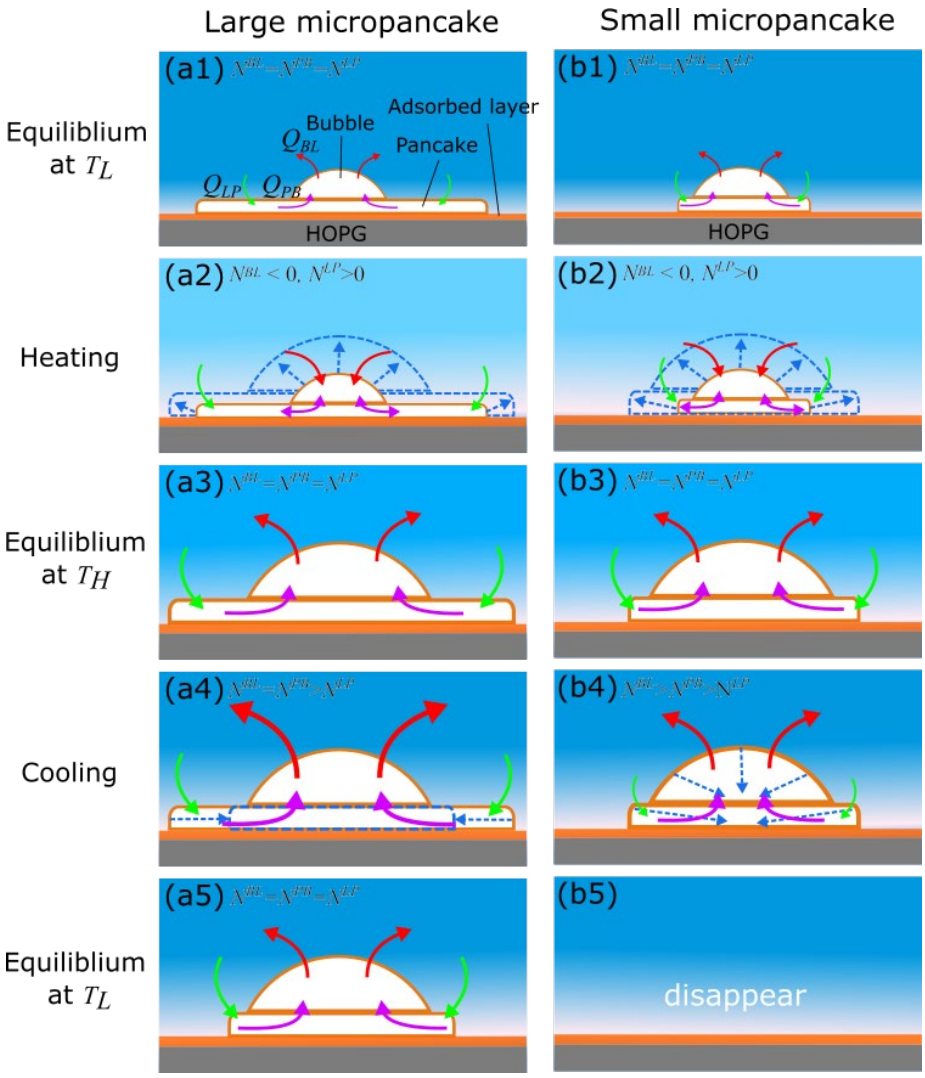

Figure 6 Schematic of nanobubbles-on-micropancakes: (a) growth and (b) dissolution by heating. (a1) and (b1) show the stationary state before heating. (a2) and (b2) show the nonstationary state during heating. (a3) and (b3) show the stationary state during heating. Images (a4) and (b4) show the nonstationary state when the water temperature decreases. Images (a5) and (b5) show the steady state when the water temperature decreased to room temperature after cooling down. The size of the arrows qualitatively indicates the strength of gas flow into and out of the nanobubbles, but not to scale. The brighter background color indicates the region that has higher gas oversaturation.

Next, we consider why heated nanobubbles lead to two results: growth and shrinkage. Consider the size of a micropancake under the surface nanobubbles (Figure 6). We assume two cases of micropancake: the comparatively larger one [Figure 6 (a1-a5)] and the comparatively smaller one [Figure 6 (b1-b5)]. We first introduce a dynamic equilibrium model[13]; the quantity of gas molecules that flows from the bottom of the nanobubble to the liquid is the same as the quantity of gas bubbles that flows from the top of the nanobubble to the liquid. On the basis of the assumption that the gas supersaturation ζ near the solid–liquid interface is a function of the distance from the solid surface to the gas molecule (because ζ depends on the interaction potential between the substrate surface and the gas molecule), one can express ζ as

$$\zeta(z,T) = \frac{\mathrm{c}_0}{c_{\mathrm{sat}}(T)} \exp\left(-\frac{\phi(z)}{k_{\mathrm{B}}T}\right) - 1 \quad (1),$$

where z is the distance between the solid surface and gas molecule, c_0 is the gas concentration outside the gas enrichment region, $c_{\mathrm{sat}}(z)$ is the saturated gas concentration, $\phi(z)$ is the solid–gas intermolecular potential, k_{B} is the Boltzmann constant, and T is absolute temperature[14,43]. $\zeta(z,T) < 0, = 0, \text{and} > 0$ indicate the undersaturated, saturated, and supersaturated states, respectively. Eq. (1) suggests the presence of a region of very high gas supersaturation at $z < \lambda$, where λ is the thickness of the gas enrichment region. In the following, ζ^{λ} and ζ represent the gas supersaturation inside and outside the gas enrichment region, respectively. The presence of the aforementioned region has been confirmed by both experiments and simulations[21,40,44–47]. Because this region functions as the supplier of gas molecules for nanobubbles, it is possible to achieve equilibrium with the gas flow caused by the high internal pressure of the nanobubbles.

Assume the nanobubble-on-micropancake—in which gas molecules flow from the

nanobubble to water, water to the micropancake, and the micropancake to the nanobubble—is in dynamic equilibrium [$N_1^{\mathrm{BL}} = N_1^{\mathrm{PB}} = N_1^{\mathrm{LP}}$; Figure 6 (a1, b1)]. We define the gas flow from the nanobubbles to water, the micropancakes to nanobubbles, and water to the micropancakes as flow in the positive direction. At room temperature ($\mathrm{T_{RT}}$) before heating, the gas supersaturation outside and inside the gas enrichment region is $\zeta_1 = 0$ and $\zeta_1^{\lambda} > 0$, respectively. Table S4 (supplementary note 5) summarizes the valuables and their relationships as per each temperature condition.

On heating, the saturated gas concentration $c_{\mathrm{sat}}(T)$ decreases, but the $\mathrm{c_0}$ value does not appreciably change because the diffusion phenomena are much slower than the temperature increase. Thus, the gas supersaturation both inside and outside the gas enrichment region increases ($\zeta_2^{\lambda} > \zeta_1^{\lambda}, \zeta_2 > \zeta_1$). This leads to flow of gas molecules from water into the nanobubbles ($N_2^{\mathrm{BL}} < 0$) and an increase in the quantity of gas molecules entering the micropancake from water ($N_2^{\mathrm{LP}} > N_1^{\mathrm{LP}}$). As a result, the equilibrium state is disrupted and thus the nanobubble, micropancake, and adsorbed layer grow [Figure 6 (a2, b2)] [40].

When the water temperature stabilizes at high temperature ($\mathrm{T_H}$), $\mathrm{c_0}$ gradually decreases and reaches $c_{\mathrm{sat}}(\mathrm{T_H})$, and the gas supersaturation outside the gas enrichment region approaches zero ($\zeta_3 = 0$). Therefore, there is no gas flow from water into the nanobubble. In contrast, the quantity of gas flow from the nanobubble to water increases because the inner pressure of the nanobubbles increases after heating [(Figure 2 and Table S2 in supplementary information)]. Additionally, because of the increase in the thickness of the adsorbed layer [Figure 5(e)]—which behaves as a solid surface[21] and is 300× denser than nitrogen gas under atmospheric pressure[20]—the solid–gas intermolecular potential $\phi(z)$ increases and thus more strongly attracts dissolved gas molecules ($\zeta_3^{\lambda} >$

ζ_1^{λ}). Consequently, the gas supersaturation inside the gas enrichment region also increases after heating. Therefore the gas flow from water to the micropancake increases ($N_3^{\mathrm{LP}} > N_1^{\mathrm{LP}}$). As a result, one reaches a dynamic equilibrium state with the entire gas phase ($N_3^{\mathrm{BL}} = N_3^{\mathrm{PB}} = N_3^{\mathrm{LP}}$) [Figure 6 (a3, b3)].

Upon a decrease in water temperature, the gas supersaturation outside the gas enrichment region becomes negative ($\zeta_4 < 0$) because of the higher saturated gas concentration c_{sat}, and the gas flow from the nanobubbles into the water increases ($N_4^{\mathrm{BL}} > N_3^{\mathrm{BL}}$). However, because the adsorbed layer is strongly adsorbed to the substrate, the constituent gas molecules do not diffuse much into the water. Thus, ϕ does not appreciably change and the gas supersaturation inside the gas enrichment does not change ($\zeta_4^{\lambda} \approx \zeta_3^{\lambda}$). Accordingly, the gas flow from the liquid to the micropancake does not change ($N_4^{\mathrm{LP}} \approx N_3^{\mathrm{LP}}$). Therefore, the dynamic equilibrium state is disrupted, but the quantity of gas molecules flowing from the micropancake to the nanobubble increases such that the nanobubbles retain their shape yet the micropancake shrinks($N_4^{\mathrm{BL}} = N_4^{\mathrm{PB}} > N_4^{\mathrm{LP}}$) [Figure 6 (a4)].

When the water temperature decreases to room temperature and stabilizes, the gas supersaturation outside the gas enrichment region approaches zero ($\zeta_5 = 0$) and the gas flow from the nanobubble surface returns to that exhibited during heating ($N_5^{\mathrm{BL}} \approx N_3^{\mathrm{BL}}$). However, because the gas supersaturation inside the gas enrichment region remains high ($\zeta_5^{\lambda} \approx \zeta_4^{\lambda}$), the gas flow from the water to the micropancake is the same as that during heating ($N_5^{\mathrm{LP}} \approx N_3^{\mathrm{LP}}$). Therefore, if there is a large micropancake before heating, the nanobubble remains stable in dynamic equilibrium ($N_5^{\mathrm{BL}} = N_5^{\mathrm{PB}} = N_5^{\mathrm{LP}}$) even after heating [Figure 6 (a5)].

Even in the case of a small micropancake [Figure 6 (b)], the phenomena from

Figure 6 (b1) to Figure 6 (b3) is the same as Figure 6 (a1) to Figure 6 (a3). However, the edge of the shrinking micropancake overlaps with the edge of the nanobubble during cooling down [Figure 6 (b4)]. As a result, N^{LP} and N^{PB} approaches zero; thus the nanobubble begins to shrink by diffusion and eventually is no longer evident [Figure 6 (b5)].

This mechanism explain the results obtained in our work. In Figure 2, the nanobubbles that had a higher inner pressure grew and the nanobubbles that had a lower inner pressure were no longer evident. Because the gas flow from a nanobubble was large when the nanobubble's inner pressure was high, the gas flow from the liquid into the micropancake must have been equally large for equilibrium. Therefore, the nanobubbles that initially had a high inner pressure were present on the (relatively) large micropancake. As a result, the nanobubbles that had a higher inner pressure grew in accordance with heating and exhibited the behavior depicted in Figure 6 (a1–a5). In contrast, the area of the micropancake underneath a nanobubble with a low inner pressure could be small because the quantity of gas molecules flowing into the nanobubble was small. Therefore, nanobubbles with low inner pressure were no longer evident during cooling down, in accordance with the mechanism shown in Figure 6 (b1–b5).

As mentioned above, the inner pressure of nanobubbles, local gas oversaturation, and the size of the micropancakes are definitely related to the growth and shrinkage of nanobubbles. However, although the size of micropancakes can be measured by AFM, there is no way to measure the local gas oversaturation near the solid-liquid interfaces. Therefore, resolving the relationships among the inner pressure, the area of micropancakes, and the local gas oversaturation and quantifying the threshold values for the occurrence of the phenomena are beyond the contents of this paper.

The proposed mechanism also reasonably explains the inconsistent behaviors reported in previous studies. Yang et al.[28] reported that surface nanobubbles grew after heating, which is consistent with our interpretation. Berkelaar et al.[30] observed that nanobubbles grew and shrank when the water temperature decreased. Shrinkage of the nanobubbles should be due to the absence of large micropancakes underlying them. We explain nanobubble growth by considering the disturbance of the AFM tip. Because we observed no micropancakes in their AFM images, we infer that the AFM tip penetrated the micropancakes and reached the bare HOPG surface in their measurements. As previously reported[48], strong scanning as per an AFM tip diffuses gas molecules in the micropancake, resulting in growth of nanobubbles in accordance with increasing ζ^{λ}.

It needs to be noted that, in the present study, we have tried to generate the gas phases by solvent exchange method 37 times. As a result, we found the gas molecule-adsorbed layer 35 times (95 %) and the micropancake 23 times (62 %), while the surface nanobubbles were generated only 5 times (14 %). We could heat the nanobubbles twice (i.e., Figure 2 and 4) out of 5 times. The number of the nanobubbles for each behavior upon heating shown in Figure 2 and 4 was summarized in Table 3.

Table 3 Number of nanobubbles for each behavior upon heating observed in Figure 2 and Figure 4.

	Before heating	1st heating			2nd heating		
Response to heating		Generation	Growth	Dissolution	Generation	Growth	Dissolution
Figure 2	44	-	32	12			
Figure 4	1	3	-	1	27	3	-

4. Conclusions

We investigated the effect of heating on surface nanobubbles by AFM imaging before and after heating. Nanobubbles in the same area exhibited divergent behaviors upon heating: generation, growth, and dissolution. Nanobubbles were evident not on the bare HOPG surface but on the previously existing micropancakes. This may be due to more thermodynamically facile formation on the existing micropancakes than heterogeneous nucleation on a bare HOPG surface. Furthermore, by simultaneously observing the surface nanobubbles and micropancake, we found that the size of the micropancake plays a key role to determine the behavior of the corresponding nanobubble on the micropancake upon heating. We proposed a possible mechanism for the behavior of heated nanobubbles. Specifically, when there was a large micropancake beneath a surface nanobubble, the nanobubble was maintained by the gas molecules from the micropancake. However, when the micropancake was small and the gas flow from the micropancake was insufficient, the dynamic equilibrium was disrupted, and the nanobubble was no longer evident. Our results will help researchers understand the nanoscopic behavior of gas phases near the solid–liquid interface in response to heating and provide valuable knowledge for modeling the mechanism of the very initial stage of onset of nucleate boiling.

Acknowledgments

This work was partially supported by JST CREST Grant No. JPMJCR18I1, JSPS KAKENHI Grant No. JP20H02089, JP20H02090, and a Grant-in-Aid for JSPS Research Fellow No. JP20J01307. The sponsors had no role in study design; in the collection, analysis and interpretation of data; in the writing of the report; and in the decision to submit the article for publication. We thank Prof. Yasuyuki Takaka, Ikuta Tatsuya, Kazuhiko Morishita, Sota Hirokawa, Riku Sakata, and Chen Kuan Ting for scientific discussions.

Supplementary material

Supplementary material associated with this article can be found in the online version.

References

[1] Y. Nam, Y.S. Ju, Bubble nucleation on hydrophobic islands provides evidence to anomalously high contact angles of nanobubbles, Appl. Phys. Lett. 93 (2008) 103115. https://doi.org/10.1063/1.2981572.

[2] B. Shen, M. Yamada, S. Hidaka, J. Liu, J. Shiomi, G. Amberg, M. Do-Quang, M. Kohno, K. Takahashi, Y. Takata, Early Onset of Nucleate Boiling on Gas-covered Biphilic Surfaces, Sci. Rep. 7 (2017) 1–15. https://doi.org/10.1038/s41598-017-02163-8.

[3] P.G. De Gennes, On Fluid/Wall Slippage, Langmuir. 18 (2002) 3413–3414. https://doi.org/10.1021/la0116342

[4] Y. Gao, J. Li, H.C. Shum, H. Chen, Drag Reduction by Bubble-Covered Surfaces Found in PDMS Microchannel through Depressurization, Langmuir. 32 (2016) 4815–4819. https://doi.org/10.1021/acs.langmuir.6b01186.

[5] Y. Wang, B. Bhushan, Boundary slip and nanobubble study in micro/nanofluidics using atomic force microscopy, Soft Matter. 6 (2009) 29–66. https://doi.org/10.1039/b917017k.

[6] H. Stevens, R.F. Considine, C.J. Drummond, R.A. Hayes, P. Attard, Effects of degassing on the long-range attractive force between hydrophobic surfaces in water, Langmuir. 21 (2005) 6399–6405. https://doi.org/10.1021/la0507535.

[7] J.L. Parker, P.M. Claesson, P. Attard, Bubbles, cavities, and the long-ranged attraction between hydrophobic surfaces, J. Phys. Chem. 98 (1994) 8468–8480. https://doi.org/10.1021/j100085a029.

[8] Q.Y. Li, R. Matsushita, Y. Tomo, T. Ikuta, K. Takahashi, Water Confined in Hydrophobic Cup-Stacked Carbon Nanotubes beyond Surface-Tension

Dominance, J. Phys. Chem. Lett. 10 (2019) 3744–3749. https://doi.org/10.1021/acs.jpclett.9b00718.

[9] X.H. Zhang, A. Quinn, W.A. Ducker, Nanobubbles at the interface between water and a hydrophobic solid, Langmuir. 24 (2008) 4756–4764. https://doi.org/10.1021/la703475q.

[10] B.M. Borkent, S.M. Dammer, H. Schönherr, G.J. Vancso, D. Lohse, Superstability of surface nanobubbles, Phys. Rev. Lett. 98 (2007) 18–21. https://doi.org/10.1103/PhysRevLett.98.204502.

[11] A. Brotchie, X.H. Zhang, Response of interfacial nanobubbles to ultrasound irradiation, Soft Matter. 7 (2011) 265–269. https://doi.org/10.1039/c0sm00731e.

[12] W.A. Ducker, Contact angle and stability of interfacial nanobubbles, Langmuir. 25 (2009) 8907–8910. https://doi.org/10.1021/la902011v.

[13] M.P. Brenner, D. Lohse, Dynamic equilibrium mechanism for surface nanobubble stabilization, Phys. Rev. Lett. 101 (2008) 1–4. https://doi.org/10.1103/PhysRevLett.101.214505.

[14] K. Yasui, T. Tuziuti, W. Kanematsu, K. Kato, Advanced dynamic-equilibrium model for a nanobubble and a micropancake on a hydrophobic or hydrophilic surface, Phys. Rev. E - Stat. Nonlinear, Soft Matter Phys. 91 (2015) 1–9. https://doi.org/10.1103/PhysRevE.91.033008.

[15] D. Lohse, X. Zhang, Pinning and gas oversaturation imply stable single surface nanobubbles, Phys. Rev. E - Stat. Nonlinear, Soft Matter Phys. 91 (2015) 1–5. https://doi.org/10.1103/PhysRevE.91.031003.

[16] J.R.T. Seddon, O. Bliznyuk, E.S. Kooij, B. Poelsema, H.J.W. Zandvliet, D. Lohse, Dynamic dewetting through micropancake growth, Langmuir. 26 (2010)

9640–9644. https://doi.org/10.1021/la101414x.

[17] X.H. Zhang, N. Maeda, J. Hu, Thermodynamic stability of interfacial gaseous states, J. Phys. Chem. B. 112 (2008) 13671–13675. https://doi.org/10.1021/jp807515f.

[18] X.H. Zhang, X. Zhang, J. Sun, Z. Zhang, G. Li, H. Fang, X. Xiao, X. Zeng, J. Hu, Detection of novel gaseous states at the highly oriented pyrolytic graphite-water interface, Langmuir. 23 (2007) 1778–1783. https://doi.org/10.1021/la062278w.

[19] L. Zhang, X. Zhang, C. Fan, Y. Zhang, J. Hu, Nanoscale multiple gaseous layers on a hydrophobic surface, Langmuir. 25 (2009) 8860–8864. https://doi.org/10.1021/la901620e.

[20] I. Schlesinger, U. Sivan, Three-Dimensional Characterization of Layers of Condensed Gas Molecules Forming Universally on Hydrophobic Surfaces, J. Am. Chem. Soc. 140 (2018) 10473–10481. https://doi.org/10.1021/jacs.8b04815.

[21] H. Teshima, Y. Takata, K. Takahashi, Adsorbed gas layers limit the mobility of micropancakes, Appl. Phys. Lett. 115 (2019) 071603. https://doi.org/10.1063/1.5113810.

[22] Y.H. Lu, C.W. Yang, I.S. Hwang, Molecular layer of gaslike domains at a hydrophobic water interface observed by frequency-modulation atomic force microscopy, Langmuir. 28 (2012) 12691–12695. https://doi.org/10.1021/la301671a.

[23] Y.H. Lu, C.W. Yang, C.K. Fang, H.C. Ko, I.S. Hwang, Interface-induced ordering of gas molecules confined in a small space, Sci. Rep. 4 (2014) 1–8. https://doi.org/10.1038/srep07189.

[24] M.G. Kang, Effect of surface roughness on pool boiling heat transfer, Int. J. Heat Mass Transf. 43 (2000) 4073–4085. https://doi.org/10.1016/S0017-9310(00)00043-0.

[25] B.J. Jones, J.P. McHale, S. V. Garimella, The influence of surface roughness on nucleate pool boiling heat transfer, J. Heat Transfer. 131 (2009) 1–14. https://doi.org/10.1115/1.3220144.

[26] L.W. Fan, J.Q. Li, L. Zhang, Z.T. Yu, K.F. Cen, Pool boiling heat transfer on a nanoscale roughness-enhanced superhydrophilic surface for accelerated quenching in water, Appl. Therm. Eng. 109 (2016) 630–639. https://doi.org/10.1016/j.applthermaleng.2016.08.131.

[27] J.S. Kim, A. Girard, S. Jun, J. Lee, S.M. You, Effect of surface roughness on pool boiling heat transfer of water on hydrophobic surfaces, Int. J. Heat Mass Transf. 118 (2018) 802–811. https://doi.org/10.1016/j.ijheatmasstransfer.2017.10.124.

[28] Y. Shangjiong, S.M. Dammer, N. Bremond, H.J.W. Zandvliet, E.S. Kooij, D. Lohse, Characterization of nanobubbles on hydrophobic surfaces in water, Langmuir. 23 (2007) 7072–7077. https://doi.org/10.1021/la070004i.

[29] X. Zhang, H. Lhuissier, C. Sun, D. Lohse, Surface nanobubbles nucleate microdroplets, Phys. Rev. Lett. 112 (2014) 1–5. https://doi.org/10.1103/PhysRevLett.112.144503.

[30] R.P. Berkelaar, J.R.T. Seddon, H.J.W. Zandvliet, D. Lohse, Temperature dependence of surface nanobubbles, ChemPhysChem. 13 (2012) 2213–2217. https://doi.org/10.1002/cphc.201100808.

[31] J. Zou, H. Zhang, Z. Guo, Y. Liu, J. Wei, Y. Huang, X. Zhang, Surface

Nanobubbles Nucleate Liquid Boiling, Langmuir. 34 (2018) 14096–14101. https://doi.org/10.1021/acs.langmuir.8b03290.

[32] X. Zhang, H. Lhuissier, O.R. Enríquez, C. Sun, D. Lohse, Deactivation of microbubble nucleation sites by alcohol-water exchange, Langmuir. 29 (2013) 9979–9984. https://doi.org/10.1021/la402015q.

[33] S.-T. Lou, Z.-Q. Ouyang, Y. Zhang, X.-J. Li, J. Hu, M.-Q. Li, F.-J. Yang, Nanobubbles on solid surface imaged by atomic force microscopy, J. Vac. Sci. Technol. B Microelectron. Nanom. Struct. 18 (2000) 2573. https://doi.org/10.1116/1.1289925.

[34] D. Lohse, X. Zhang, Surface nanobubbles and nanodroplets, Rev. Mod. Phys. 87 (2015) 981–1035. https://doi.org/10.1103/RevModPhys.87.981.

[35] R.P. Berkelaar, E. Dietrich, G.A.M. Kip, E.S. Kooij, H.J.W. Zandvliet, D. Lohse, Exposing nanobubble-like objects to a degassed environment, Soft Matter. 10 (2014) 4947–4955. https://doi.org/10.1039/c4sm00316k.

[36] H. Teshima, T. Nishiyama, K. Takahashi, Nanoscale pinning effect evaluated from deformed nanobubbles, J. Chem. Phys. 146 (2017) 014708. https://doi.org/10.1063/1.4973385.

[37] H. Teshima, K. Takahashi, Y. Takata, T. Nishiyama, Wettability of AFM tip influences the profile of interfacial nanobubbles, J. Appl. Phys. 123 (2018) 054303. https://doi.org/10.1063/1.5010131.

[38] S.R. German, X. Wu, H. An, V.S.J. Craig, T.L. Mega, X. Zhang, Interfacial nanobubbles are leaky: Permeability of the gas/water interface, ACS Nano. 8 (2014) 6193–6201. https://doi.org/10.1021/nn5016049.

[39] J.B. Park, D. Shin, S. Kang, S.P. Cho, B.H. Hong, Distortion in Two-

Dimensional Shapes of Merging Nanobubbles: Evidence for Anisotropic Gas Flow Mechanism, Langmuir. 32 (2016) 11303–11308. https://doi.org/10.1021/acs.langmuir.6b01672.

[40] H. Teshima, N. Nakamura, Q.Y. Li, Y. Takata, K. Takahashi, Zigzag gas phases on holey adsorbed layers, RSC Adv. 10 (2020) 44854–44859. https://doi.org/10.1039/d0ra08861g.

[41] S. Yang, E.S. Kooij, B. Poelsema, D. Lohse, H.J.W. Zandvliet, Correlation between geometry and nanobubble distribution on HOPG surface, Epl. 81 (2008) 64006. https://doi.org/10.1209/0295-5075/81/64006.

[42] L. Wang, X. Wang, L. Wang, J. Hu, C.L. Wang, B. Zhao, X. Zhang, R. Tai, M. He, L. Chen, L. Zhang, Formation of surface nanobubbles on nanostructured substrates, Nanoscale. 9 (2017) 1078–1086. https://doi.org/10.1039/c6nr06844h.

[43] B.H. Tan, H. An, C.D. Ohl, Stability, Dynamics, and Tolerance to Undersaturation of Surface Nanobubbles, Phys. Rev. Lett. 122 (2019) 134502. https://doi.org/10.1103/PhysRevLett.122.134502.

[44] H. Peng, M.A. Hampton, A. V. Nguyen, Nanobubbles do not sit alone at the solid-liquid interface, Langmuir. 29 (2013) 6123–6130. https://doi.org/10.1021/la305138v.

[45] H. Teshima, Q.Y. Li, Y. Takata, K. Takahashi, Gas molecules sandwiched in hydration layers at graphite/water interfaces, Phys. Chem. Chem. Phys. 22 (2020) 13629–13636. https://doi.org/10.1039/d0cp01719a.

[46] T.H. Yen, Y.L. Chen, C.H. Lin, Effects of gas adsorption and surface conditions on interfacial nanobubbles, Langmuir. 37 (2021) 2759-2770. https://doi.org/10.1021/acs.langmuir.0c03511.

[47] Y.X. Chen, Y.L. Chen, T.H. Yen, Investigating Interfacial Effects on Surface Nanobubbles without Pinning Using Molecular Dynamics Simulation, Langmuir. 34 (2018) 15360–15369. https://doi.org/10.1021/acs.langmuir.8b03016.

[48] D. Li, B. Zeng, Y. Wang, Probing the “Gas Tunnel” between Neighboring Nanobubbles, Langmuir. 35 (2019) 15029–15037. https://doi.org/10.1021/acs.langmuir.9b02682.